

1 **Correction of Systematic Model Forcing Bias of CLM using**
2 **Assimilation of Cosmic-Ray Neutrons and Land Surface**
3 **Temperature: a study in the Heihe Catchment, China**

4
5 Xujun Han^{1,2,3}

- 6 1. Cold and Arid Regions Environmental and Engineering Research Institute,
7 Chinese Academy of Sciences, Lanzhou, Gansu 730000, PR China
8 2. Forschungszentrum Jülich, Agrosphere (IBG 3), Leo-Brandt-Strasse, 52425 Jülich,
9 Germany
10 3. Centre for High-Performance Scientific Computing in Terrestrial Systems: HPSC
11 TerrSys, Geoverbund ABC/J, Leo-Brandt-Strasse, 52425 Jülich, Germany
12

13 Harrie-Jan Hendricks Franssen^{1,2}

- 14 1. Forschungszentrum Jülich, Agrosphere (IBG 3), Leo-Brandt-Strasse, 52425 Jülich,
15 Germany
16 2. Centre for High-Performance Scientific Computing in Terrestrial Systems: HPSC
17 TerrSys, Geoverbund ABC/J, Leo-Brandt-Strasse, 52425 Jülich, Germany
18

19 Rafael Rosolem

20 Department of Civil Engineering, University of Bristol, Bristol BS8 1TR, UK
21

22 Rui Jin

23 Cold and Arid Regions Environmental and Engineering Research Institute, Chinese
24 Academy of Sciences, Lanzhou, Gansu 730000, PR China
25

26 Xin Li

27 Cold and Arid Regions Environmental and Engineering Research Institute, Chinese
28 Academy of Sciences, Lanzhou, Gansu 730000, PR China
29

30 Harry Vereecken^{1,2}

- 31 1. Forschungszentrum Jülich, Agrosphere (IBG 3), Leo-Brandt-Strasse, 52425 Jülich,
32 Germany
33 2. Centre for High-Performance Scientific Computing in Terrestrial Systems: HPSC
34 TerrSys, Geoverbund ABC/J, Leo-Brandt-Strasse, 52425 Jülich, Germany
35
36
37
38

39 Corresponding author: Xujun Han, Cold and Arid Regions Environmental and
40 Engineering Research Institute, Chinese Academy of Sciences, Lanzhou, Gansu
41 730000, PR China. (hanxj@lzb.ac.cn)
42

43 **Abstract**

44 The recent development of the non-invasive cosmic-ray soil moisture sensing
45 technique fills the gap between point scale soil moisture measurements and regional
46 scale soil moisture measurements by remote sensing. A cosmic-ray probe measures
47 soil moisture for a footprint with a diameter of ~600 m (at sea level) and with an
48 effective measurement depth between 12 cm to 76 cm, depending on the soil humidity.
49 In this study, it was tested whether neutron counts also allow to correct for a
50 systematic error in the model forcings. Lack of water management data often cause
51 systematic input errors to land surface models. Here, the assimilation procedure was
52 tested for an irrigated corn field (Heihe Watershed Allied Telemetry Experimental
53 Research - HiWATER, 2012) where no irrigation data were available as model input
54 although for the area a significant amount of water was irrigated. In the study, the
55 measured cosmic-ray neutron counts and Moderate Resolution Imaging
56 Spectroradiometer (MODIS) land surface temperature (LST) products were jointly
57 assimilated into the Community Land Model (CLM) with the Local Ensemble
58 Transform Kalman Filter. Different data assimilation scenarios were evaluated, with
59 assimilation of LST and/or cosmic-ray neutron counts, and possibly parameter
60 estimation of leaf area index (LAI). The results show that the direct assimilation of
61 cosmic-ray neutron counts can improve the soil moisture and evapotranspiration (ET)
62 estimation significantly, correcting for lack of information on irrigation amounts. The
63 joint assimilation of neutron counts and LST could improve further the ET estimation,
64 but the information content of neutron counts exceeded the one of LST. Additional

65 improvement was achieved by calibrating LAI, which after calibration was also closer
66 to independent field measurements. It was concluded that assimilation of neutron
67 counts was useful for ET and soil moisture estimation even if the model has a
68 systematic bias like neglecting irrigation. However, also the assimilation of LST
69 helped to correct the systematic model bias introduced by neglecting irrigation and
70 LST could be used to update soil moisture with state augmentation.

71 **Keywords:** Cosmic-ray neutron counts, Land surface temperature, Evapotranspiration,
72 Land data assimilation, Parameter estimation

73 **1. Introduction**

74 Soil moisture plays a key role for crop and plant growth, water resources
75 management and land surface-atmosphere interaction. Therefore accurate soil
76 moisture retrieval is important. Point scale measurements can be obtained by methods
77 like time domain reflectometry (TDR) (Robinson et al., 2003) and larger scale, coarse
78 soil moisture information from remote sensing sensors (Entekhabi et al., 2010; Kerr et
79 al., 2010). Wireless Sensor Networks (WSN) allow characterization of soil moisture at
80 the catchment scale with many local connected sensors at separated locations (Bogena
81 et al., 2010). TDR only measures the point scale soil moisture and the maintenance of
82 WSN is expensive. Recently, neutron count intensity measured by above-ground
83 cosmic-ray probes was proposed as alternative information source on soil moisture.
84 Neutron count intensity is measured non-invasively at an intermediate scale between
85 the point scale and the coarse remote sensing scale (Zreda et al., 2008). A network of
86 cosmic-ray sensors (CRS) has been set-up over N-America (Zreda et al., 2012).

87 Cosmic rays are composed of primary protons mainly. The fast neutrons
88 generated by high-energy neutrons colliding with nuclei lead to “evaporation” of fast
89 neutrons and the generated and moderated neutrons in the ground can diffuse back
90 into the air where their intensity can be measured by the cosmic-ray soil moisture
91 probe. Soil moisture affects the rate of moderation of fast neutrons, and controls the
92 neutron concentration and the emission of neutrons into the air. Dry soils have low
93 moderating power and are highly emissive; wet soils have high moderating power and
94 are less emissive. The neutrons are mainly moderated by the hydrogen atoms

95 contained in the soil water and emitted to the atmosphere where the neutrons mix
96 instantaneously at a scale of hundreds of meters. The measurement area of a
97 cosmic-ray soil moisture probe represents a circle with a diameter of ~600 m at sea
98 level (Desilets and Zreda, 2013) and the measurement depth decreases non-linearly
99 from ~76 cm (dry soils) to ~12 cm (saturated soils) (Zreda et al., 2008). The measured
100 cosmic-ray neutron counts show an inverse correlation with soil moisture content. The
101 cosmic-ray neutron intensity could be reduced to 60% of surface cosmic-ray neutron
102 intensity if the soil moisture was increased from zero to 40% (Zreda et al., 2008). The
103 soil moisture estimation on the basis of cosmic-ray probe based neutron counts over a
104 horizontal footprint of hectometers received considerable attention in scientific
105 literature during the last years (Desilets et al., 2010; Zreda et al., 2008; Zreda et al.,
106 2012).

107 Hydrogen atoms are present as water in the soil, lattice soil water, below ground
108 biomass, atmospheric water vapor, snow water, above ground biomass, intercepted
109 water by vegetation and water on the ground. These additional hydrogen sources
110 contribute to the measured neutron intensity. The role of these additional hydrogen
111 sources should be included in the analysis of the cosmic-ray measurements in order to
112 isolate the main contribution from soil moisture. Formulations for handling water
113 vapor (Rosolem et al., 2013), for lattice water and organic carbon (Franz et al., 2013)
114 and for a litter layer present on the soil surface (Bogena et al., 2013) have been
115 developed.

116 The positive impact of soil moisture data assimilation was shown in several

117 studies. Importantly, surface soil moisture could be used to obtain better
118 characterization of the root zone soil moisture (Barrett and Renzullo, 2009; Crow et
119 al., 2008; Das et al., 2008; Draper et al., 2011; Li et al., 2010). It was also shown that
120 the assimilation of soil moisture observations can be used to correct rainfall errors
121 (Crow et al., 2011; Yang et al., 2009). Often a systematic bias between measured and
122 modelled soil moisture content can be found; soil moisture estimation can be
123 significantly improved using joint state and bias estimation (De Lannoy et al., 2007;
124 Kumar et al., 2012; Reichle, 2008). Also studies on data assimilation of remotely
125 sensed land surface temperature products show a positive impact on the estimation of
126 soil moisture, latent heat flux and sensible heat flux (Ghent et al., 2010; Xu et al.,
127 2011). Also in these studies it was found that bias, in these cases soil temperature bias,
128 of land surface models can be removed with land surface temperature assimilation
129 (Bosilovich et al., 2007; Reichle et al., 2010). Other studies updated both land surface
130 model states and parameters with soil moisture and land surface temperature data
131 (Bateni and Entekhabi, 2012; Han et al., 2014a; Montzka et al., 2013; Pauwels et al.,
132 2009). The assimilation of measured cosmic-ray neutron counts in a land surface
133 model was successfully tested, but these studies focused on state updating alone
134 (Rosolem et al., 2014; Shuttleworth et al., 2013). In this paper we focus on the
135 assimilation of measured cosmic-ray neutron counts for improving soil moisture
136 content characterization at the field scale. This paper focuses on the case that model
137 input is biased. Land surface models still are affected by limited knowledge on water
138 resources management and for regions in China (and elsewhere) typically no

139 information on irrigation amounts is available as irrigation is mainly by the flooding
140 system. We analyse whether measured neutron counts are able to correct for such
141 biases. This case is not only relevant for neglecting irrigation in China, but also for
142 other water resources management issues (e.g., groundwater pumping) which are
143 neglected in the simulations. Neglecting irrigation in land surface models results in a
144 large bias in the simulated soil moisture content because of a lack of water input. The
145 bias in soil moisture content also results in a too small latent heat flux and too high
146 sensible heat flux. We hypothesize that data assimilation also can play an important
147 role for removing such biases in data deficient areas. One possible strategy in data
148 assimilation studies for handling this type of bias, which is not followed in this paper,
149 is to calibrate the simulation model (e.g., land surface model) prior to data
150 assimilation to remove biases (Kumar et al., 2012) and use the corrected simulation
151 model in the context of sequential data assimilation. A different strategy was followed
152 in this paper and no a priori bias correction was carried out because this type of
153 problem (neglecting water resources management) does not allow for such an a priori
154 bias correction. The bias can be attributed to the model structure, model parameters,
155 atmospheric forcing or observation data, and the bias-aware assimilation requires the
156 assumption that the bias comes from a particular source. If the source of bias is not
157 attributed to the right source, model predictions cannot be improved (Dee, 2005).
158 Therefore bias-blind assimilation in which the bias estimation was not handled
159 explicitly was used for safety. Instead, it was investigated whether neutron counts
160 measured by cosmic-ray probe were able to correct for the bias. Aim is to improve the

161 soil moisture profile estimation in a crop land with seed corn as main crop type.

162 In CLM, land surface fluxes are calculated based on the Monin-Obukhov
163 similarity theory. The sensible heat flux is formulated as a function of temperature and
164 LAI, and the latent heat flux is formulated as a function of the temperature and leaf
165 stomatal resistances. The leaf stomatal resistance is calculated from the Ball-Berry
166 conductance model (Collatz et al., 1991). The updates of soil temperature and
167 vegetation temperature are derived based on the solar radiation absorbed by top soil
168 (or vegetation), longwave radiation absorbed by soil (or vegetation), sensible heat flux
169 from soil (or vegetation) and latent heat flux from soil (or vegetation). Measured land
170 surface temperature is composed of the ground temperature and vegetation
171 temperature. Therefore a difference between measured and calculated land surface
172 temperature can be adjusted by changing land surface fluxes. As land surface fluxes
173 are sensitive to soil moisture content, land surface temperature is sensitive to soil
174 moisture content.

175 Therefore, the land surface temperature (LST) products measured by the
176 Moderate Resolution Imaging Spectroradiometer (MODIS) Terra (MOD11A1) and
177 Aqua (MYD11A1) are also assimilated jointly to improve the soil temperature profile
178 estimation because the evapotranspiration is sensitive to the soil temperature. Two
179 Terra LST products can be obtained per day at 10:30 am/pm and two Aqua LST
180 products can be obtained per day at 1:30 am/pm. Soil moisture, land surface
181 temperature and LAI influence the estimation of latent and sensible heat fluxes
182 (Ghilain et al., 2012; Jarlan et al., 2008; Schwinger et al., 2010; van den Hurk, 2003;

183 Yang et al., 1999), and therefore this study focuses in addition on the calibration of
184 LAI with help of the assimilation of land surface temperature. However, there are
185 large discrepancies between the remotely retrieved LAI and measured values, and the
186 MODIS LAI product underestimates in situ measured LAI by 44% on average
187 (<http://landval.gsfc.nasa.gov/>), and therefore the LAI is also calibrated by data
188 assimilation. In summary, the novel aspects of this work are: 1) investigating whether
189 data assimilation is able to correct for missing water resources management data
190 without a priori bias correction; 2) joint assimilation of cosmic-ray neutron counts,
191 LST and updating of LAI; 3) application of this framework to real-world data in an
192 irrigated area with the availability of detailed verification data.

193

194 **2. Materials and Methods**

195 **2.1 Study Area and Measurement**

196 The Heihe River Basin is the second largest inland river basin of China, and it is
197 located between 97.1° E- 102.0° E and 37.7° N- 42.7° N and covers an area of
198 approximately 143,000 km² (Li et al., 2013). In 2012, a multi-scale observation
199 experiment of evapotranspiration with a well-equipped superstation (Daman
200 superstation) to measure the atmospheric forcings and soil moisture at 2 cm, 4 cm, 10
201 cm, 20 cm, 40 cm, 80 cm, 120 cm and 160 cm depth (Xu et al., 2013), was carried out
202 from June to September in the framework of the Heihe Watershed Allied Telemetry
203 Experimental Research (HiWATER) (Li et al., 2013). SoilNet wireless network nodes
204 (Bogena et al., 2010) were deployed to measure soil moisture content and soil

205 temperature at four layers (4 cm, 10 cm, 20 cm and 40 cm). One cosmic-ray soil
206 moisture probe (CRS-1000B) was installed (Han et al., 2014b) with 23 SoilNet nodes
207 (Jin et al., 2014; Jin et al., 2013) in the footprint (Fig. 1). The main crop type within
208 the footprint of the cosmic-ray probe is seed corn. The irrigation is applied through
209 channels using the flooding irrigation method. Exact amounts of applied irrigation are
210 therefore not available.

211 The measured cosmic-ray neutron count data were processed to remove the
212 outliers according to the sensor voltage (≤ 11.8 Volt) and relative humidity ($\geq 80\%$).
213 The surface fluxes were measured using the eddy covariance technique, and data were
214 processed using EdiRe (<http://www.geos.ed.ac.uk/abs/research/micromet/EdiRe>)
215 software, in which the anemometer coordinate rotation, signal lag removal, frequency
216 response correction, density corrections and signal de-spiking were done for the raw
217 data. The energy balance closure was not considered in this study. The LAI was
218 measured by the LAI-2000 scanner during the field experiment, there are 17 samples
219 collected in 14 days of 3 months.

220 [\[Insert Figure 1 here\]](#)

221

222 **2.2 Land Surface Model and Data**

223 The CLM was used to simulate the spatio-temporal distribution of soil moisture,
224 soil temperature, land surface temperature, vegetation temperature, sensible heat flux,
225 latent heat flux and soil heat flux of the study area. The coupled water and energy
226 balance are modeled in CLM, and the land surface heterogeneity is represented by

227 patched plant functional types and soil texture (Oleson et al., 2013).

228 The soil properties used in CLM were from the soil database of China with 1 km
229 spatial resolution (Shangguan et al., 2013). The MODIS 500 m resolution plant
230 functional type product (MCD12Q1) (Sun et al., 2008) which was resampled by
231 nearest neighbor interpolation to 1 km resolution and MODIS LAI product
232 (MCD15A3) with 1 km spatial resolution (Han et al., 2012) were used as input. Due
233 to a lack of measurement data, two atmospheric forcing data sets were used: the
234 Global Land Data Assimilation System reanalysis data (Rodell et al., 2004) was
235 interpolated using the National Centers for Environmental Prediction (NCEP) bilinear
236 interpolation library iplib in spatial and temporal dimensions and used in the CLM for
237 the spin-up period (http://www.nco.ncep.noaa.gov/pmb/docs/libs/ipilib/ncep_ipilib.shtml).
238 For the three months data assimilation period, hourly forcing data (incident
239 longwave radiation, incident solar radiation, precipitation, air pressure, specific
240 humidity, air temperature and wind speed) from the Daman superstation of HiWATER
241 were available and used.

242

243 **2.3 Cosmic-Ray Forward Model**

244 In this study, the new developed COsmic-ray Soil Moisture Interaction Code
245 (COSMIC) model (Shuttleworth et al., 2013) was used as the cosmic-ray forward
246 model to simulate the cosmic-ray neutron count rate using the soil moisture profile as
247 input. The effective measurement depth of the cosmic-ray soil moisture probe ranges
248 from 12 cm (wet soils) to 76 cm (dry soils) (Zreda et al., 2008), within which 86% of

249 the above-ground measured neutrons originate. COSMIC also calculates the effective
 250 sensor depth based on the cosmic-ray neutron intensity and the soil moisture profile
 251 values (Franz et al., 2012; Shuttleworth et al., 2013).

252 COSMIC makes several assumptions to calculate the number of fast neutrons
 253 reaching the cosmic-ray soil moisture probe (N_{COSMOS}) at a near-surface measurement
 254 location, and the soil layer with a depth of 3 meters for the complete soil profile, was
 255 discretized into 300 layers for the integration of Eq. 2 in COSMIC. The number of
 256 fast neutrons reaching the cosmic-ray probe N_{COSMOS} is formulated as (Shuttleworth
 257 et al., 2013):

$$258 \quad N_{COSMOS} = N \int_0^{\infty} \left\{ A(z) [\alpha \rho_s(z) + \rho_w(z)] \exp \left(- \left[\frac{m_s(z)}{L_1} + \frac{m_w(z)}{L_2} \right] \right) \right\} dz \quad (1)$$

$$259 \quad A(z) = \left(\frac{2}{\pi} \right)^{\pi/2} \int_0^{\pi/2} \exp \left(\frac{-1}{\cos(\theta)} \left[\frac{m_s(z)}{L_3} + \frac{m_w(z)}{L_4} \right] \right) d\theta \quad (2)$$

$$260 \quad \alpha = 0.405 - 0.102 \times \rho_s \quad (3)$$

$$261 \quad L_3 = -31.76 + 99.38 \times \rho_s \quad (4)$$

262 where N is the high energy neutron intensity (counts/hour), z denotes the soil
 263 layer depth (m), ρ_s the dry soil bulk density (g/cm^3), ρ_w the total water density,
 264 including the lattice water (g/cm^3) and α denotes the ratio of fast neutron creation
 265 factor. L_1 is the high energy soil attenuation length with value of 162.0 g/cm^2 and
 266 L_2 the high energy water attenuation length of 129.1 g/cm^2 . In equation (2) θ is the
 267 angle between the vertical below the detector and the line between the detector and
 268 each point in the plane, $m_s(z)$ and $m_w(z)$ are the integrated mass per unit area of
 269 dry soil and water (g/cm^2), respectively. L_3 denotes the fast neutron soil attenuation

270 length (g/cm^2) and L_4 stands for the fast neutron water attenuation length with value
271 of $3.16 \text{ g}/\text{cm}^2$.

272 The cosmic-ray neutron intensity reaching the land surface is influenced by air
273 pressure, atmospheric water vapor content and incoming neutron flux. In order to
274 isolate the contribution of soil moisture content to the measured neutron density, it is
275 important to take these effects into account and the calibrated neutron count intensity
276 can be derived as follows:

$$277 \quad N_{\text{Corr}} = N_{\text{Obs}} \times f_p \times f_{\text{wv}} \times f_i \quad (5)$$

278 where N_{Corr} represents corrected neutron counts and N_{Obs} the measured
279 neutron counts. f_p is the correction factor for air pressure, f_{wv} the correction
280 factor for atmospheric water vapor and f_i the correction factor for incoming neutron
281 flux.

282 The correction factor for air pressure f_p can be calculated as (Zreda et al.,
283 2012):

$$284 \quad f_p = \exp\left(\frac{P - P_0}{L}\right) \quad (6)$$

285 where P (mbar) is the local air pressure, P_0 (mbar) the average air pressure
286 during the measurement period and L (g/cm^2) is the mass attenuation length for
287 high-energy neutrons; the default value of $128 \text{ g}/\text{cm}^2$ was used in this study (Zreda et
288 al., 2012).

289 The correction factor f_{wv} for atmospheric water vapor is calculated as (Rosolem
290 et al., 2013):

$$291 \quad f_{\text{wv}} = 1 + 0.0054 \times (\rho_{\text{v}0} - \rho_{\text{v}0}^{\text{ref}}) \quad (7)$$

292 where ρ_{v0} (k/gm³) is the absolute humidity at the measurement time and ρ_{v0}^{ref}
293 (kg/m³) is the average absolute humidity during the measurement period.

294 Fluctuations in the incoming neutron flux should be removed because the
295 cosmic-ray probe is designed to measure the neutron flux based on the incoming
296 background neutron flux. The correcting factor f_i for the incoming neutron flux is
297 calculated as:

$$298 \quad f_i = \frac{N_m}{N_{avg}} \quad (8)$$

299 where N_m is the measured incoming neutron flux and N_{avg} is the average
300 incoming neutron flux during the measurement period. The measured data at the
301 Jungfrauoch station in Switzerland at 3560 m (<http://cosray.unibe.ch/>) was used to
302 calculate N_m and N_{avg} . The temporal (secular or diurnal) variations caused by the
303 sunspot cycle could be removed after this correction (Zreda et al., 2012).

304 In this study, the soil moisture for the CRS footprint scale was calculated from the
305 arithmetic mean of the 23 SoilNet soil moisture observations. The calibration of the
306 high energy neutron intensity parameter N in equation (1) was done using the
307 measured cosmic-ray neutron counts rate and averaged soil moisture content at the
308 CRS footprint scale. Because lattice water was unknown for this site, a value of 3%
309 was assumed in this study (Franz et al., 2012). Hourly soil moisture measurements for
310 a period of 2.5 months were used for COSMIC calibration. Inside the cosmic-ray
311 probe footprint, the amount of applied irrigation was spatially variable due to the
312 different management practice of each farmer. The gradient search algorithm
313 L-BFGS-B (Zhu et al., 1997) was used to minimize the root mean square error of the

314 differences between simulated cosmic-ray neutron counts (using measured soil
315 moisture by SoilNet as input to COSMIC) and the measured neutron counts N_{Corr} .
316 The optimized parameter value of N was 615.96 counts/hour in this case.

317 The simulated soil moisture content for 10 CLM soil layers (3.8 m depth) was
318 used as input to COSMIC in order to simulate the corresponding neutron count
319 intensity and compare it with the measured neutron count intensity. It should be
320 mentioned that it is unlikely that anything beyond 1 m deep will substantially impact
321 the results because the effective measurement depth of the cosmic-ray probe is
322 between 12 and 76 cm. The COSMIC model assumes a more detailed soil profile.
323 COSMIC interpolates the soil moisture information from the ten CLM soil layers to
324 information for 300 soil layers of depth 1cm. The contribution of each soil layer to the
325 measured neutron flux will change temporally depending on the soil moisture
326 condition. Therefore the effective measurement depth of the cosmic ray probe will
327 also change temporally. COSMIC calculates the vertically weighted soil moisture
328 content based on the vertical distribution of soil moisture content.

329

330 **2.4 Two Source Formulation - TSF**

331 The land surface temperature products of MODIS are composed of a ground
332 temperature and vegetation temperature component, which are however unknown.
333 CLM models the ground temperature and vegetation temperature separately, but does
334 not model the composed land surface temperature as seen by MODIS. The
335 corresponding land surface temperature of CLM should therefore be modelled for

336 data assimilation purposes. The two source formulation (Kustas and Anderson, 2009)
 337 was used in this study to calculate the land surface temperature from the MODIS view
 338 angle using ground temperature and vegetation temperature simulated by CLM:

$$339 \quad T_s = [F_c(\Phi)T_c^4 + (1 - F_c(\Phi)T_g^4)]^{1/4} \quad (9)$$

340 where T_s (K) is the composed surface temperature as seen by the MODIS sensor,
 341 $F_c(\Phi)$ is the fraction vegetation cover observed from the sensor view angle Φ
 342 (radians), T_c (K) is the vegetation temperature and T_g (K) is the ground temperature.
 343 (Kustas and Anderson, 2009):

$$344 \quad F_c(\Phi) = 1 - \exp\left(\frac{-0.5\Omega(\Phi)LAI}{\cos\Phi}\right) \quad (10)$$

345 where LAI is the leaf area index, $\Omega(\Phi)$ is a clumping index to represent the
 346 nonrandom leaf area distributions of farmland or other heterogeneous land surfaces
 347 (Anderson et al., 2005), and is defined as:

$$348 \quad \Omega(\Phi) = \frac{0.49\Omega_{\max}}{0.49 + (\Omega_{\max} - 0.49)\exp(k\theta^{3.34})} \quad (11)$$

$$349 \quad \Omega_{\max} = 0.49 + 0.51(\sin\Phi)^{0.05} \quad (12)$$

$$350 \quad k = -\{0.3 + [1.7 * 0.49 * (\sin\Phi)^{0.1}]^{14}\} \quad (13)$$

351

352 **2.5 Assimilation Approach**

353 The Local Ensemble Transform Kalman Filter (LETKF) was used as the
 354 assimilation algorithm, which is one of the square root variants of the ensemble
 355 Kalman filter (Evensen, 2003; Hunt et al., 2007; Miyoshi and Yamane, 2007). The
 356 model uncertainties are represented using the ensemble simulation of model states and
 357 LETKF derives the background error covariance using the model state ensemble

358 members. LETKF uses the non-perturbed observations to update all the ensemble
359 members of model states at each assimilation step.

360 In this study, x_1^b, \dots, x_N^b denote the model state ensemble members; \bar{x}^b is the
361 ensemble mean of x_1^b, \dots, x_N^b ; N is the ensemble size; y_1^b, \dots, y_N^b denote the mapped
362 model state ensemble members; \bar{y}^b is the ensemble mean of y_1^b, \dots, y_N^b ; H is the
363 observation operator (COSMIC for soil moisture or the two source function for land
364 surface temperature). The analysis step of LETKF can be summarized as follows:

365 Prepare the model state vector X^b :

$$366 \quad X^b = [x_1^b - \bar{x}^b, \dots, x_N^b - \bar{x}^b] \quad (14)$$

367 where \bar{x}^b is composed of one vertically weighted soil moisture content and soil
368 moisture content for 10 CLM-layers, resulting in a state dimension equal to 11 if only
369 the neutron count observation was assimilated; and \bar{x}^b is composed of surface
370 temperature, ground temperature, vegetation temperature and soil temperature for 15
371 CLM-layers if only the land surface temperature observations were assimilated
372 without soil moisture update, giving a state dimension of 18. The water and energy
373 balance are coupled, and in CLM the energy balance is firstly solved, then the derived
374 surface fluxes are used for updating soil moisture content. The cross correlation
375 between the soil temperature and soil moisture can be calculated using the ensemble
376 prediction in LETKF, and this makes the updating of soil moisture by assimilating
377 land surface temperature possible. We also used the land surface temperature to
378 update the soil moisture profile, in this case the soil moisture vector was augmented to
379 the LETKF state vector of land surface temperature assimilation, resulting in a state

380 dimension of 28. For the calibration of the LAI, the state vector was augmented with
 381 surface temperature, ground temperature, vegetation temperature, soil temperature for
 382 15 CLM-layers and LAI if only the land surface temperature observations were
 383 assimilated without soil moisture update. This resulted then in a state dimension of
 384 19.

385 Construct the mapped model state vector Y^b after transformation of observation
 386 operator:

$$387 \quad y_i^b = H(x_i^b) \quad (15)$$

$$388 \quad Y^b = [y_1^b - \bar{y}^b, \dots, y_N^b - \bar{y}^b] \quad (16)$$

389 The following analysis is looped for each model grid cell to calculate the update
 390 of model state ensemble members:

391 Calculate analysis error covariance matrix P^a :

$$392 \quad P^a = [(N - 1)I + Y^{bT} R^{-1} Y^b] \quad (17)$$

393 The perturbations in ensemble space are calculated as:

$$394 \quad W^a = [(N - 1)P^a]^{1/2} \quad (18)$$

395 Calculate the analysis mean \bar{w}^a in ensemble space and add to each column of
 396 W^a to get the analysis ensemble in ensemble space:

$$397 \quad \bar{w}^a = P^a Y^{bT} R^{-1} (y^o - \bar{y}^b) \quad (19)$$

398 Calculate the new analysis:

$$399 \quad X^a = X^b [\bar{w}^a + W^a] + \bar{x}^b \quad (20)$$

400 where R is the observation error covariance matrix, y^o is the observation vector
 401 and X^a contains the updated model ensemble members.

402 The LETKF method can also be extended to do parameter estimation using a state
403 augmentation approach (Bateni and Entekhabi, 2012; Li and Ren, 2011; Moradkhani
404 et al., 2005; Nie et al., 2011). Alternative strategies for parameter estimation are a dual
405 approach (Moradkhani et al., 2005) with separate updating of states and parameters.
406 Vrugt et al. (2005) also proposed a dual approach with parameter updating in an outer
407 optimization loop using a Markov Chain Monte Carlo method, and state updating in
408 an inner loop. The a priori calibration of model parameters is also an option (Kumar et
409 al., 2012). With the augmentation approach, the state vector of LETKF can be
410 augmented by the parameter vector including soil properties (sand fraction, clay
411 fraction and organic matter density) and vegetation parameters (LAI, etc.). In a
412 preliminary sensitivity study it was found that for this site simulation results were
413 more sensitive to the LAI than to soil properties. Soil texture is also quite well known
414 for this site from measurements. Therefore in this study, only the LAI was in some of
415 the simulation scenarios calibrated. In the different scenarios of land surface
416 temperature assimilation, the LETKF state vector was also augmented to include LAI
417 as calibration target. As a consequence, the augmented state vector contains surface
418 temperature, ground temperature, and vegetation temperature, 15 layers of soil
419 temperature and LAI, making up a state dimension equal to 19 for the scenarios of
420 land surface temperature assimilation without soil moisture update; for the scenarios
421 of land surface temperature with soil moisture update, the state dimension is 29. The
422 10 layers of soil moisture and 15 layers of soil temperature are the standard CLM
423 layout for both soil moisture and soil temperature. The hydrology calculations are

424 done over the top 10 layers, and the bottom 5 layers are specified as bedrock. The
425 lower 5 layers are hydrologically inactive layers. Temperature calculations are done
426 over all layers (Oleson et al., 2013).

427

428 **3. Experiment Setup**

429 First the 50 ensemble members of CLM with perturbed soil properties and
430 atmospheric forcing data were driven from the 1st of Jan. 2012 to the 31st of May 2012
431 to do the CLM spin-up; second an additional assimilation period of cosmic-ray
432 neutron counts was done from the 1st of Jun. 2012 to the 30th Aug. 2012 to reduce the
433 spin-up error. Then the final CLM states on 30th Aug. 2012 were used as the initial
434 states for the following data assimilation scenarios. Perturbed soil properties were
435 generated by adding a spatially uniform perturbation sampled from a uniform
436 distribution between -10% and 10% to the values extracted from the Soil Database of
437 China for Land Surface Modeling (1 km spatial resolution). The LAI was perturbed
438 with multiplicative uniform distributed random noise in the range of [0.8~1.2]. The
439 perturbations added to the model forcings show correlations in space and time. The
440 spatial correlation was induced by a Fast Fourier Transform and the temporal
441 correlation by a first-order auto-regressive model (Han et al., 2013; Kumar et al.,
442 2009; Reichle et al., 2010). The statistics on the perturbation of the forcing data are
443 summarized in Table 1. The values of standard deviations and temporal correlations in
444 Table 1 were chosen based on previous catchment scale and regional scale data
445 assimilation studies (De Lannoy et al., 2012; Kumar et al., 2012; Reichle et al., 2010).

446 [\[Insert Table 1 here\]](#)

447 The cosmic-ray neutron intensity was assimilated every 3 days at 12Z from the 1st
448 of June 2012 onwards, because we found that the difference between daily
449 assimilation and 3 days assimilation was small (Entekhabi et al., 2010; Kerr et al.,
450 2010). The measured neutron count intensity showed large temporal fluctuations in
451 time and these fluctuations were not corresponding to the temporal variations of soil
452 moisture. Therefore the measured neutron count intensity was smoothed with the
453 Savitzky–Golay filter using a moving average window of size 31 hours and a
454 polynomial of order 4 (Savitzky and Golay, 1964). The originally measured neutron
455 counts and smoothed neutron counts are plotted in Fig. 2. The assimilation frequency
456 of MODIS LST products of MOD11A1 and MYD11A1 was up to 4 times (maximum)
457 per day depending on the data availability. There are 230 observation data (including
458 cosmic-ray probe neutron counts, MODIS LST, MOD11A1 and MYD11A1 LST) in
459 the whole assimilation window. The variance of the instantaneous measured neutron
460 intensity is equal to the measured neutron count intensity (Zreda et al., 2012) and
461 smaller for temporal averaging for daily or sub-daily applications. The instantaneous
462 neutron intensity was assimilated in this study. The variance of MODIS LST was
463 assumed to be 1 K (Wan and Li, 2008).

464 The 4 days MODIS LAI product was aggregated and used as the CLM LAI
465 parameter. Because the LAI from MODIS is usually lower than the true value
466 (compared with the field measured LAI in the HiWATER experiment) and because the
467 surface flux and surface temperature are sensitive to the LAI, two additional scenarios

468 were investigated where LAI was calibrated to study the impact of LAI estimation on
469 surface flux estimation within the data assimilation framework.

470 The following assimilation scenarios were compared: (1) CLM: open loop
471 simulation without assimilation; (2) Only_CRS: only the measured neutron counts
472 were assimilated; (3) Only_LST: only the MODIS LST products were assimilated.
473 The quality control flags of LST products were used to select the data with good
474 quality for assimilation; (4) CRS_LST: the measured neutron counts and MODIS LST
475 products were assimilated jointly. In the above scenarios, the neutron count data was
476 used to update the soil moisture and the LST data were used to update the ground
477 temperature, vegetation temperature and soil temperature. (5) LST_Feedback: We also
478 evaluated the scenario of assimilating the LST measurements to update the soil
479 moisture profile. (6) CRS_LST_Par_LAI: the LAI was included as variable to be
480 calibrated, otherwise the scenario was the same as CRS_LST. (7)
481 LST_Feedback_Par_LAI: the LAI was included as variable to be calibrated,
482 otherwise the scenario was the same as LST_Feedback. (8) CRS_LST_True_LAI: the
483 in situ measured LAI during the HiWATER experiment was used in the model
484 simulation.

485 [\[Insert Figure 2 here\]](#)

486

487 **4. Results and Discussion**

488 In order to evaluate the assimilation results for the different scenarios outlined in
489 section 3, the Root Mean Square Error (RMSE) was used:

490
$$\text{RMSE} = \sqrt{\frac{\sum_{n=i}^N (\text{Estimated} - \text{Measured})^2}{N}} \quad (21)$$

491 where “*Estimated*” is the ensemble mean without assimilation or the ensemble
492 mean after assimilation, “*Measured*” is measured soil moisture content evaluated at
493 the SoilNet nodes (or latent heat flux, sensible heat flux or soil heat flux). N is the
494 number of time steps. For the soil moisture analysis in this study, N is equal to 2184.
495 The smaller the RMSE value is, the closer assimilation results are to measured values,
496 which is in general considered to be desirable.

497 The temporal evolution of soil moisture content at 10, 20, 50 and 80 cm depth for
498 different scenarios is plotted in Fig. 3 and Fig. 4. The RMSE values for different
499 scenarios are summarized in Table 2. Assimilating the land surface temperature could
500 improve the soil moisture profile estimation in the scenario of
501 LST_Feedback_Par_LAI; the soil moisture results are better than the open loop run at
502 all depths. With the assimilation of CRS neutron counts, the soil moisture RMSE
503 values (scenarios CRS_LST_Par_LAI and CRS_LST_True_LAI) decreased
504 significantly. The RMSE values for the scenarios Only_CRS and CRS_LST (not
505 shown) are similar to CRS_LST_Par_LAI, which indicates that the main
506 improvement for the soil moisture profile characterization is achieved by neutron
507 count assimilation; and land surface temperature assimilation and LAI estimation play
508 a minor role. Without assimilation of cosmic-ray probe neutron counts, the soil
509 moisture simulation cannot be improved (scenario Only_LST). However, the
510 scenarios of LST_Feedback and LST_Feedback_Par_LAI improve the soil moisture
511 profile characterization, which shows that explicitly using LST to update soil moisture

512 content in the data assimilation routine gives better results than using LST only to
513 update soil moisture by the model equations. Results of LST_Feedback and
514 LST_Feedback_Par_LAI are similar; therefore only results for
515 LST_Feedback_Par_LAI are shown in Fig. 3 and Fig. 4. This implies that the
516 improved soil moisture characterization due to LAI calibration is low. The results for
517 the cosmic-ray probe neutron count assimilation proved that the cosmic-ray probe
518 sensor can be used to improve the soil moisture profile estimation at the footprint
519 scale.

520 [\[Insert Figure 3 here\]](#)

521 [\[Insert Figure 4 here\]](#)

522 [\[Insert Table 2 here\]](#)

523 Fig. 5 depicts the scatter plots of measured ET versus modelled ET for different
524 scenarios, and the accumulated ET for all scenarios are summarized in the lower-right
525 corner of Fig. 5. The EC measured evapotranspiration (ET) is 384.7 mm for the
526 assimilation period, without energy balance closure correction. The true
527 evapotranspiration is therefore likely larger, but not much larger as the energy balance
528 gap was limited (3.7%). The CLM estimated ET, without data assimilation, using only
529 precipitation as input is 223.7 mm and is much smaller than the measured value as
530 applied irrigation is not considered in the model. This open loop simulated value
531 would imply water stress and a limitation of canopy transpiration and soil evaporation
532 due to low soil moisture content. Assimilation of land surface temperature only
533 (Only_LST) hardly affected the estimated ET and was not able to correct for the

534 artificial water stress condition. However, if land surface temperature was used to
535 update soil moisture directly, taking into account correlations between the two states
536 in the data assimilation routine, the ET estimates improved to 336.8 mm and 354.8
537 mm for the scenarios of LST_Feedback and LST_Feedback_Par_LAI respectively.
538 The assimilation of land surface temperature of MODIS with soil moisture update
539 results in significant improvements of ET.

540 The different neutron count assimilation scenarios also resulted in significantly
541 improved estimates of ET. Univariate assimilation of cosmic-ray neutron data
542 (Only_CRS) resulted in 301.9 mm ET. This shows that the impact of neutron count
543 assimilation to correct evapotranspiration estimates is little smaller than the impact of
544 land surface temperature with soil moisture update. Joint assimilation of land surface
545 temperature data and cosmic-ray neutron data (CRS_LST) gave a slightly larger ET of
546 310.6 mm than Only_CRS. Scenarios of CRS_LST_Par_LAI and
547 CRS_LST_True_LAI gave the best ET estimates (360.5 mm and 349.3 mm). This
548 shows that correcting the biased LAI-estimates from MODIS by in situ data or
549 calibration helped to improve model estimates.

550 [\[Insert Figure 5 here\]](#)

551 The RMSE values of latent heat flux, sensible heat flux and soil heat flux for all
552 scenarios are summarized in Fig. 6. It is obvious that the RMSE values are very large
553 for both the latent heat flux (123.9 W/m²) and sensible heat flux (80.5 W/m²) for the
554 open loop run and all other scenarios where the soil moisture was not updated. If the
555 land surface temperature was assimilated to update the soil moisture, the latent heat

556 flux RMSE decreased to 60.5 W/m^2 (LST_Feedback) and 62.5 W/m^2
557 (LST_Feedback_Par_LAI). The scenario where soil moisture and LAI are jointly
558 updated (LST_Feedback_Par_LAI) gave worse results than the scenario of
559 LST_Feedback. Again, the assimilation of neutron counts also resulted in a strong
560 RMSE reduction for the latent heat flux (76.5 W/m^2 for Only_CRS). If in addition
561 land surface temperature was assimilated and LAI optimized, the RMSE value of
562 latent heat flux further decreased to 56.1 W/m^2 (70.7 W/m^2 without LAI optimization).
563 If the field measured LAI was used instead in the assimilation (CRS_LST_True_LAI),
564 the RMSE was 61.0 W/m^2 . These results are in correspondence with the ones
565 discussed before for soil moisture characterization. Evidently, the combined
566 assimilation of cosmic-ray probe neutron counts and land surface temperature, and
567 calibration of LAI (or use of field measured LAI as model input) shows the strongest
568 improvement for the estimation of land surface fluxes. The soil heat flux did not show
569 a clear improvement related to assimilation and showed only some improvement in
570 case LAI was calibrated. For the scenario of land surface temperature assimilation
571 without soil moisture update (Only_LST), estimates of latent and sensible heat flux
572 are not improved. It means that under water stress condition, the improved
573 characterization of land surface temperature (and soil temperature) does not contribute
574 to a better estimation of land surface fluxes.

575 [\[Insert Figure 6 here\]](#)

576 The updated LAI for scenarios of LST_Feedback_Par_LAI and
577 CRS_LST_Par_LAI is shown in Fig. 7. The MODIS LAI product was used as input

578 for CLM and time series are plotted as blue line in Fig. 7 (Background). The LAI was
579 also measured in the HiWATER experiment, and the measured values are shown as
580 green star (Observation). Ens_Mean represents the mean LAI of all ensemble
581 members (Ensembles). It is obvious that MODIS underestimates the LAI compared
582 with the observations. With the assimilation of land surface temperature, the LAI
583 could be updated and be closer to the observations, but there is still a significant
584 discrepancy between the measured LAI and the updated one. The LAI values for the
585 scenario with LAI calibration (CRS_LST_Par_LAI) are close to the measured LAI
586 values (CRS_LST_True_LAI), which is an encouraging result. The calibrated LAI
587 shows some unrealistic increases and decreases during the assimilation period, which
588 is inherent to the data assimilation approach. A smoothed representation of the LAI
589 might provide a more realistic picture.

590 [\[Insert Figure 7 here\]](#)

591 This study illustrates that for an irrigated farmland, the measured cosmic-ray
592 probe neutron counts can be used to improve the soil moisture profile estimation
593 significantly. Without irrigation data, CLM underestimated soil moisture content. The
594 cosmic-ray neutron count data assimilation can be used as an alternative way to
595 retrieve the soil moisture content profile in CLM. The improved soil moisture
596 simulation was helpful for the characterization of the land surface fluxes. The
597 univariate assimilation of land surface temperature without soil moisture update is not
598 helpful for the estimation of land surface fluxes and even worsened the sensible heat
599 flux characterization (Fig. 6). However, in a multivariate data assimilation framework

600 where land surface temperature was assimilated together with measured cosmic-ray
601 probe neutron counts, the land surface temperature assimilation contributed
602 significantly to an improved ET estimation. The simulated canopy transpiration in
603 CLM was in general too low, even when the water stress condition was corrected by
604 assimilating neutron counts, which was related to small values of the LAI. The
605 additional estimation of LAI through the land surface temperature assimilation
606 resulted in an increase of the LAI yielding an increase of estimated ET.

607 In general, land surface models need to be calibrated before use in land data
608 assimilation, especially if there is an apparent large bias in the model simulation (Dee,
609 2005). The simulation of soil moisture and surface fluxes was biased in our study,
610 mainly due to the lack of irrigation water as input. This bias cannot be corrected a
611 priori without exact irrigation data, which are not available in the field. The data
612 assimilation was proven to be an efficient way to remove the model bias in this case.
613 We also calculated the equivalent water thickness to analyze the equivalent irrigated
614 water after each step of soil moisture update. For the scenarios of CRS_LST_Par_LAI
615 and CRS_LST_True_LAI, the equivalent irrigation in three months was 693.6 mm
616 and 607.6 mm, respectively. Because the irrigation method is flood irrigation, it is not
617 easy to evaluate the true irrigation applied in the field. From the results we see
618 however that the applied irrigation (in the model) is much larger than actual ET
619 (~600-700mm vs ~400mm). This could indicate that the amount of applied irrigation
620 in the model is too large, but irrigation by flooding is also inefficient and results in
621 excess runoff and infiltration to the groundwater, because it cannot be controlled so

622 well as sprinkler irrigation or drip irrigation. Therefore, the calculated amount of
623 irrigation could be realistic, but might also be too large if soil properties are erroneous
624 in the model.

625 The soil moisture content measured by the cosmic-ray probe represents the depth
626 between 12 cm (very humid) and 76 cm (extremely dry case) depending on the
627 amount of soil water (soil moisture content and lattice water). Therefore the effective
628 sensor depth of the cosmic-ray probe will change over time. In order to model the
629 variable sensor depth and the relationship between the soil moisture content and
630 neutron counts, the new developed COSMIC model was used as the observation
631 operator in this study. Additionally the influences of air pressure, atmospheric vapor
632 pressure and incoming neutron counts were removed from the original measured
633 neutron counts. Because there is still some water in the crop which also affects the
634 cosmic-ray probe sensor, the COSMIC observation operator could be improved to
635 include vegetation effects. Several default parameters proposed by (Shuttleworth et al.,
636 2013) were used in the COSMIC model, these parameters probably need further
637 calibration following the development of the COSMIC model.

638 The spatial distribution of soil moisture for the study area was very
639 heterogeneous due to the small farmland patches and different irrigation periods for
640 the different farmlands. Therefore the soil moisture content inferred by SoilNet may
641 not represent the true soil moisture content of the cosmic-ray probe footprint, which is
642 a further limitation of this study. Although the Cosmic-ray Soil Moisture Observing
643 System (COSMOS) has been designed as a continental scale network by installing

644 500 COSMOS probes across the USA (Zreda et al., 2012), there are still some
645 disadvantages of COSMOS compared with remote sensing. COSMOS is also
646 expensive for extensive deployment to measure the continental/regional scale soil
647 moisture.

648 **5. Summary and Conclusions**

649 In this paper, we studied the univariate assimilation of MODIS land surface
650 temperature products, the univariate assimilation of measured neutron counts by the
651 cosmic-ray probe, the bivariate assimilation of land surface temperature and neutron
652 count data, and the additional calibration of LAI for an irrigated farmland at the Heihe
653 catchment in China, where data on the amount of applied irrigation were lacking. The
654 most important objective of this study was to test whether data assimilation is able to
655 correct for the absence of information on water resources management as model input,
656 a situation commonly encountered in large scale land surface modelling. For the
657 specific case of lacking irrigation data, no prior bias correction is possible. The bias
658 blind assimilation without explicit bias estimation was used. We focused on the model
659 bias introduced by the forcing data and the LAI, and neglected the other sources of
660 bias. In case LAI was calibrated, this was done at each data assimilation step of land
661 surface temperature. The data assimilation experiments were carried out with the
662 CLM and the data assimilation algorithm used was the LETKF. A likely further model
663 bias, besides missing information on irrigation, is the underestimation of LAI by
664 MODIS, which was used to force the model.

665 The results show that the direct assimilation of measured cosmic-ray neutron

666 counts improves the estimation of soil moisture significantly, whereas univariate
667 assimilation of land surface temperature without soil moisture update does not
668 improve soil moisture estimation. However, if the land surface temperature was
669 assimilated to update the soil moisture profile directly with help of the state
670 augmentation method, the evapotranspiration and soil moisture could be improved
671 significantly. This result suggests that the land surface temperature remote sensing
672 products are needed to correct the characterization of the soil moisture profile and the
673 evapotranspiration. The improved soil moisture estimation after the assimilation of
674 neutron counts resulted in a better ET estimation during the irrigation season,
675 correcting the too low ET of the open loop simulation. The joint assimilation of
676 neutron counts and MODIS land surface temperature improved the ET estimation
677 further compared to neutron count assimilation only. The best ET estimation was
678 obtained for the joint assimilation of cosmic-ray neutron counts, MODIS land surface
679 temperature including calibration of the LAI (or if field measured LAI was used as
680 input). This shows that bias due to neglected information on water resources
681 management can be corrected by data assimilation if a combination of soil moisture
682 and land surface temperature data is available.

683 We can conclude that data assimilation of neutron counts and land surface
684 temperature is useful for ET and soil moisture estimation of an irrigated farmland,
685 even if irrigation data are not available and excluded from model input. The land
686 surface temperature measurements are an alternative data source to improve the soil
687 moisture and land surface fluxes estimation under water stress conditions. This shows

688 the potential of data assimilation to correct also a systematic model bias. LAI
689 optimization further improves simulation results, which is also likely related to a
690 systematic underestimation of LAI by the MODIS remote sensing product. The results
691 of using the calibrated LAI are comparable to the results of using field measured LAI
692 as model input.

693

694 **Acknowledgements**

695 This work is supported by the NSFC (National Science Foundation of China)
696 project (grant number: 41271357, 91125001), the Knowledge Innovation Program of
697 the Chinese Academy of Sciences (grant number: KZCX2-EW-312) and the
698 Transregional Collaborative Research Centre 32, financed by the German Science
699 foundation. Jungfraujoch neutron monitor data were kindly provided by the
700 Cosmic-ray Group, Physikalisches Institut, University of Bern, Switzerland. We
701 acknowledge computing resources and time on the Supercomputing Center of Cold
702 and Arid Region Environment and Engineering Research Institute of Chinese
703 Academy of Sciences.

704

705 **List of Tables**

706 Table 1 Summary of perturbation parameters for atmospheric forcing data.

707

708 Table 2 Root Mean Square Error (RMSE) of soil moisture profile of open loop run
709 (CLM), feedback assimilation of land surface temperature including LAI calibration
710 (LST_Feedback_Par_LAI), bivariate assimilation of neutron counts and land surface
711 temperature including LAI calibration (CRS_LST_Par_LAI) and bivariate
712 assimilation of neutron counts and land surface temperature (CRS_LST_True_LAI).

713

714

Table 1 Summary of perturbation parameters for atmospheric forcing data

Variables	Noise	Standard deviation	Time Correlation scale	Spatial Correlation Scale	Cross correlation
Precipitation	Multiplicative	0.5	24 h	5 km	[1.0,-0.8, 0.5, 0.0,
Shortwave radiation	Multiplicative	0.3	24 h	5 km	-0.8, 1.0,-0.5, 0.4,
Longwave radiation	Additive	20 W/m ²	24 h	5 km	0.5, -0.5, 1.0, 0.4,
Air temperature	Additive	1 K	24 h	5 km	0.0, 0.4, 0.4, 1.0]

716

717

718 Table 2 Root Mean Square Error (RMSE) of soil moisture profile of open loop run
 719 (CLM), feedback assimilation of land surface temperature including LAI calibration
 720 (LST_Feedback_Par_LAI), bivariate assimilation of neutron counts and land surface
 721 temperature including LAI calibration (CRS_LST_Par_LAI) and bivariate
 722 assimilation of neutron counts and land surface temperature using ground-based
 723 measured LAI as input (CRS_LST_True_LAI).

Soil Layer Depth	RMSE (m ³ /m ³)			
	Open Loop (CLM)	LST_Feedback _Par_LAI	CRS_LST _Par_LAI	CRS_LST _True_LAI
10 cm	0.202	0.137	0.085	0.086
20 cm	0.167	0.106	0.047	0.048
50 cm	0.193	0.112	0.112	0.119
80 cm	0.188	0.124	0.136	0.146

724

725

726 **List of Figures**

727 Figure 1. Map of the cosmic-ray probe and SoilNet Nodes in the footprint of the CRS
728 probe positioned at the Heihe river catchment

729

730 Figure 2. Measured and temporally smoothed CRS neutron counts

731

732 Figure 3. Soil moisture at 10 cm (upper) and 20 cm (lower) depth as obtained from an
733 open loop run (CLM), local sensors (Obs), and different simulation scenarios. For a
734 description of the scenarios see section 3 of the paper. The CRS neutron counts were
735 assimilated from the 1st of June

736

737 Figure 4. Same as figure 3 but for 50 cm and 80 cm.

738

739 Figure 5. Evapotranspiration estimated according different scenarios for the period
740 June-August 2012. For a full description see Fig. 3.

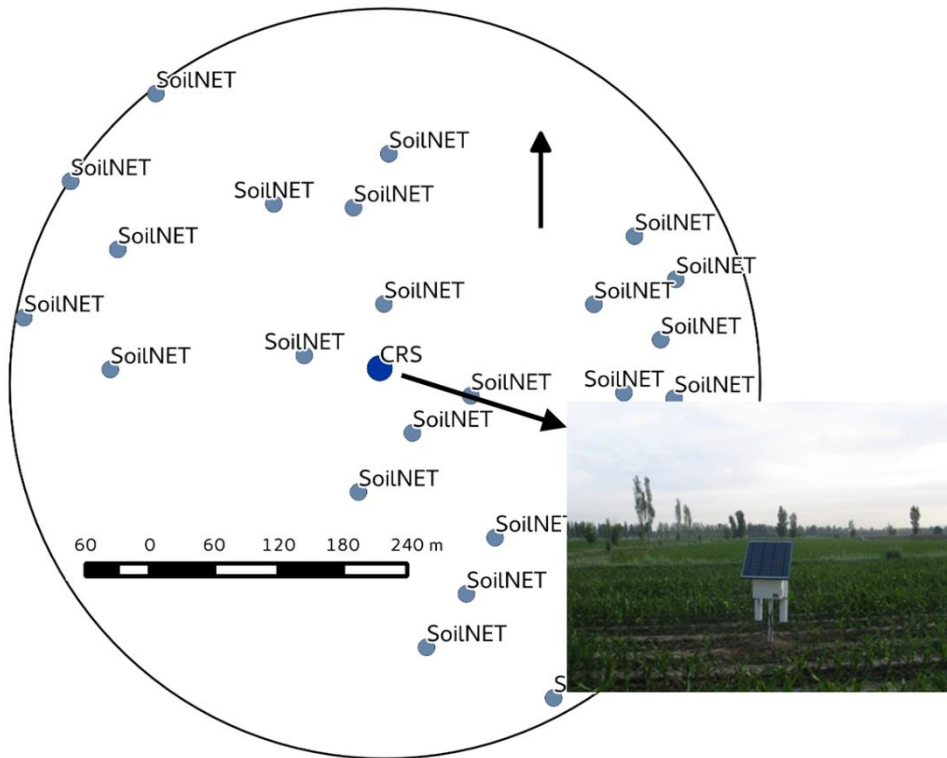
741

742 Figure 6. RMSE values of latent heat flux, sensible heat flux and soil heat flux for the
743 period June-August 2012. For a description of the scenarios see section 3 of the paper.

744

745 Figure 7. LAI evolution for the period June-August 2012. Displayed are the measured
746 LAI (Observation), default values (Background), mean of ensemble members
747 (Ens_Mean) and ensemble members (Ensembles) for scenarios of
748 LST_Feedback_Par_LAI (upper) and CRS_LST_Par_LAI (lower)

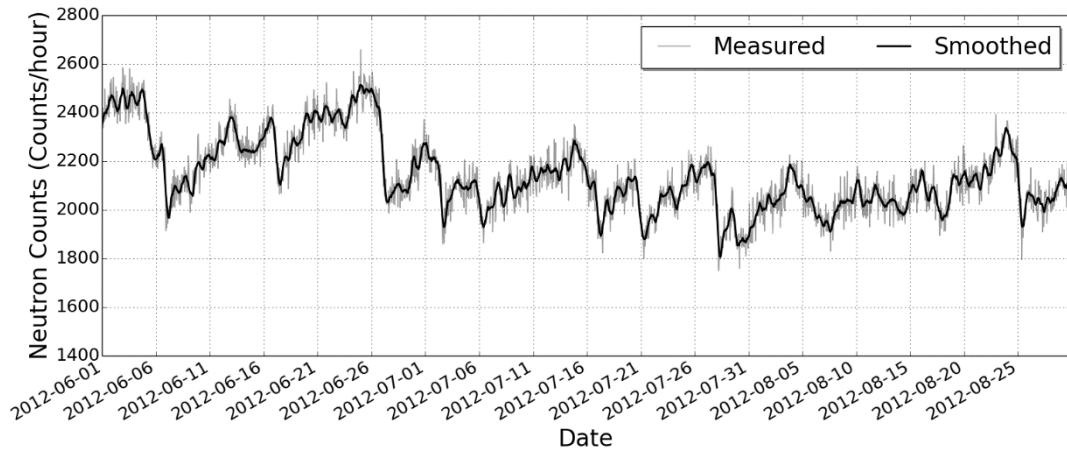
749



750

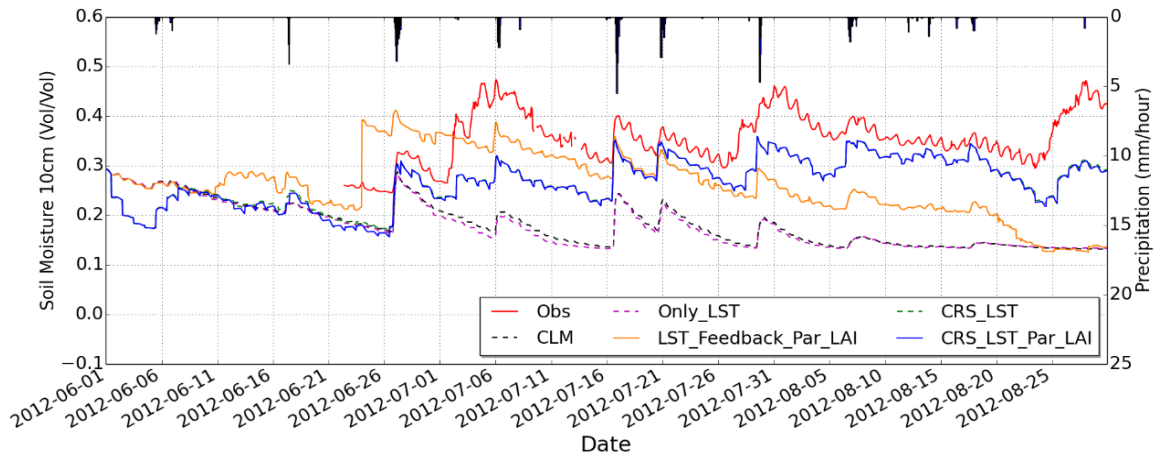
751 Figure 1. Map of the cosmic-ray probe and SoilNet Nodes in the footprint of the CRS
 752 probe positioned at the Heihe river catchment

753

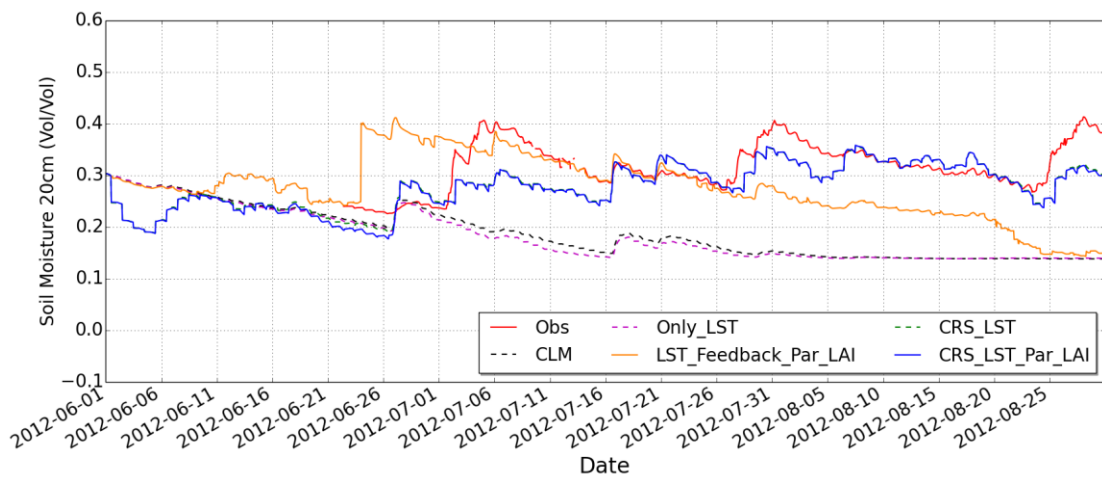


754
755
756

Figure 2. Measured and temporally smoothed CRS neutron counts

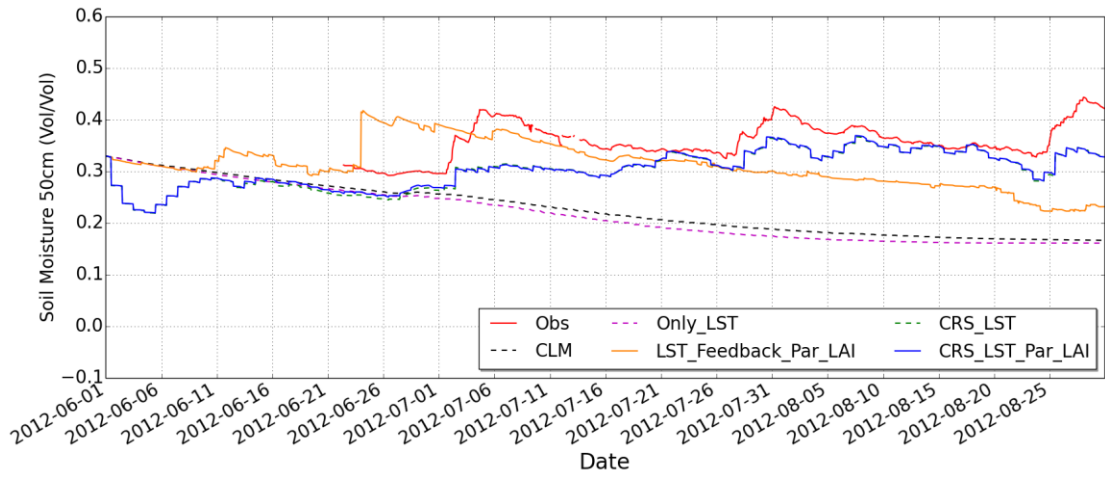


757

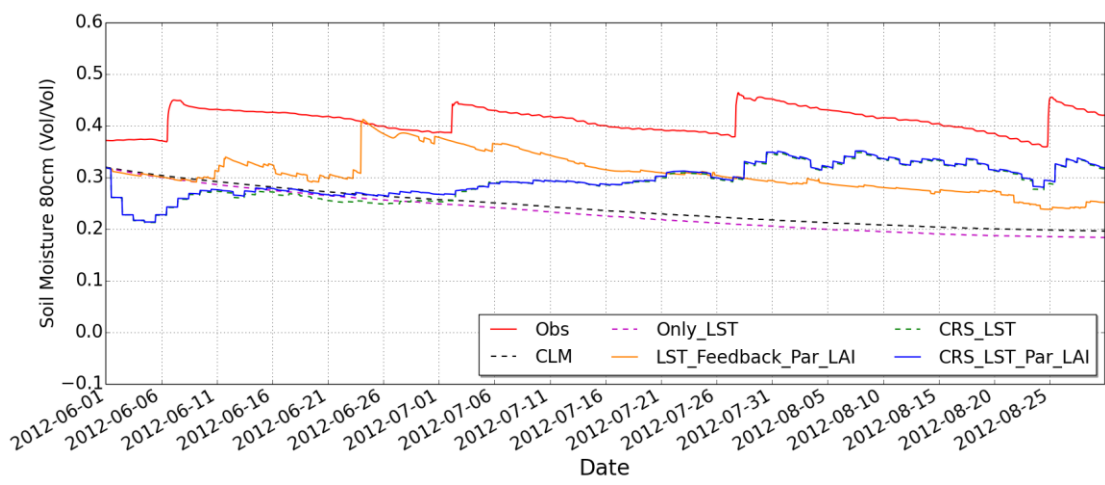


758

759 Figure 3. Soil moisture at 10 cm (upper) and 20 cm (lower) depth as obtained from an
 760 open loop run (CLM), local sensors (Obs), and different simulation scenarios. For a
 761 description of the scenarios see section 3 of the paper. The CRS neutron counts were
 762 assimilated from the 1st of June onwards.
 763



764



765

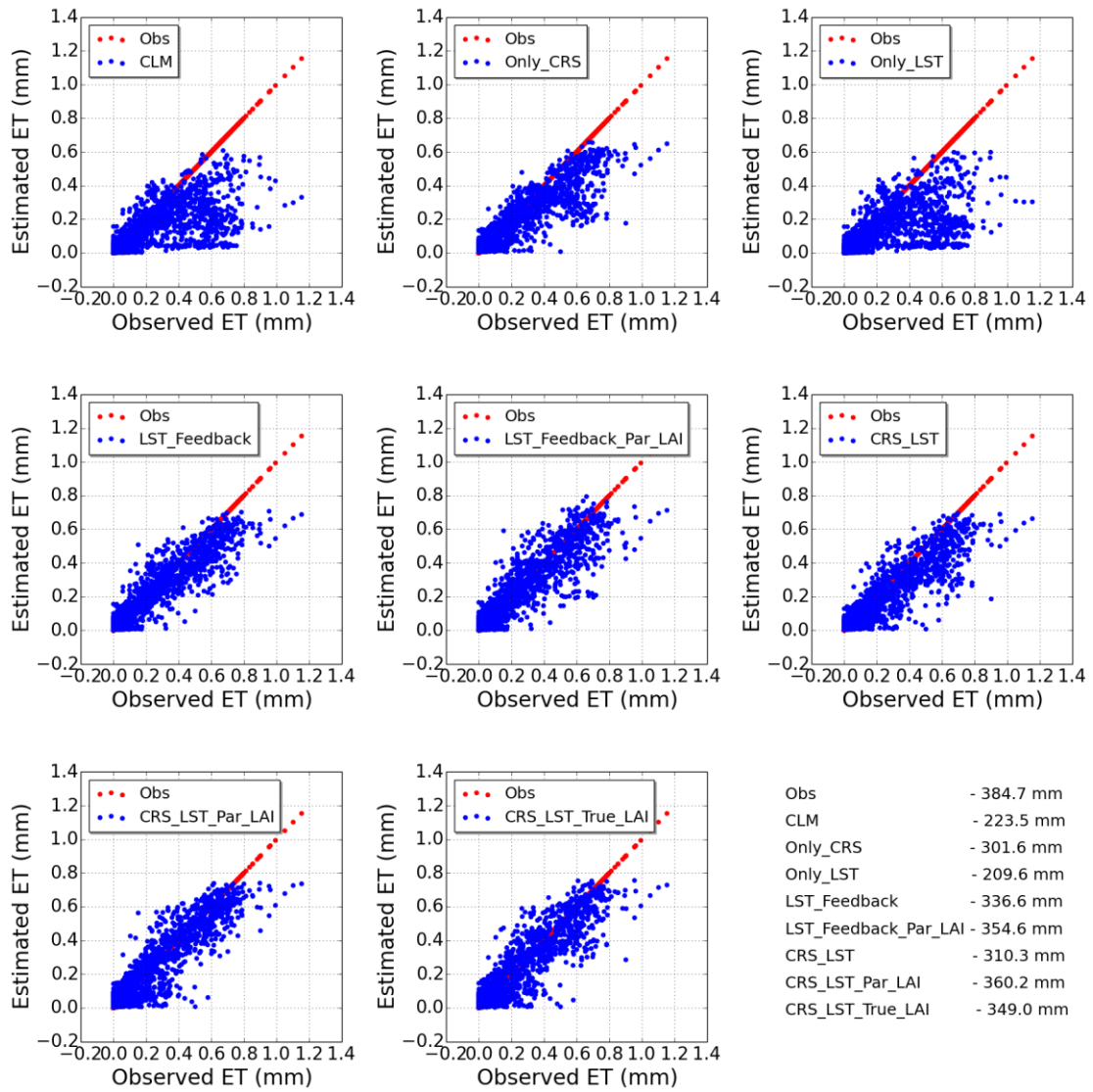
766

767

768

769

Figure 4. Same as figure 3 but for 50 cm and 80 cm.



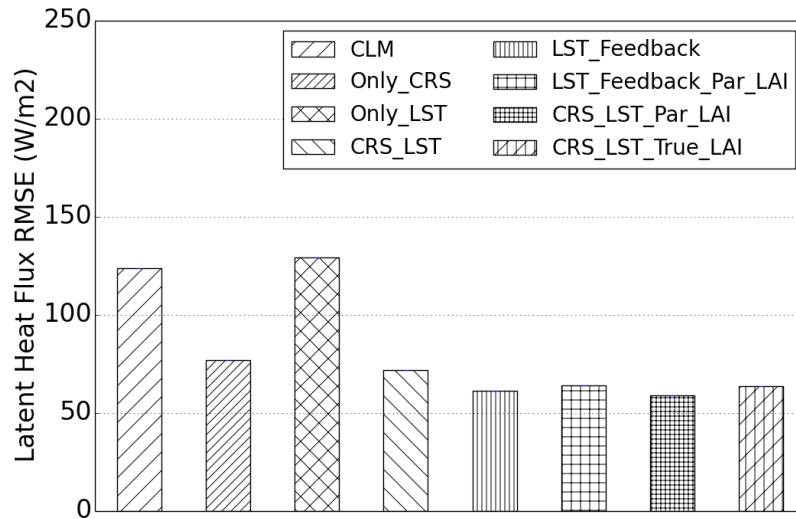
770

771

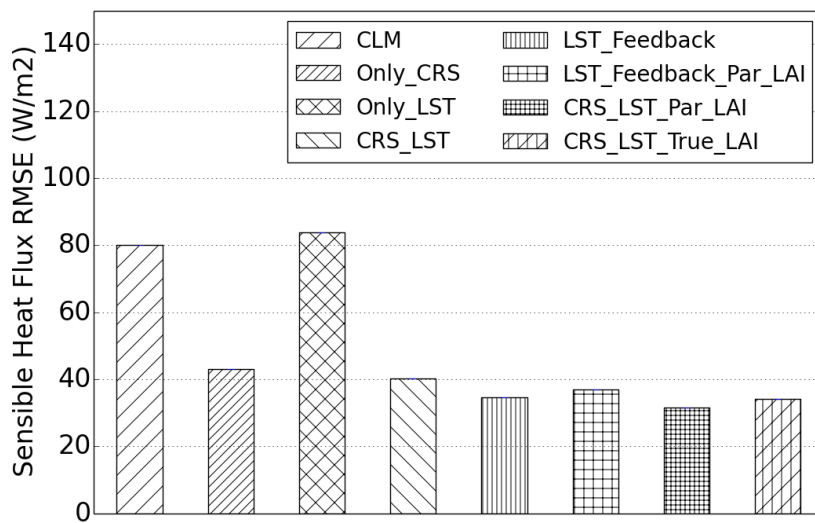
772

773

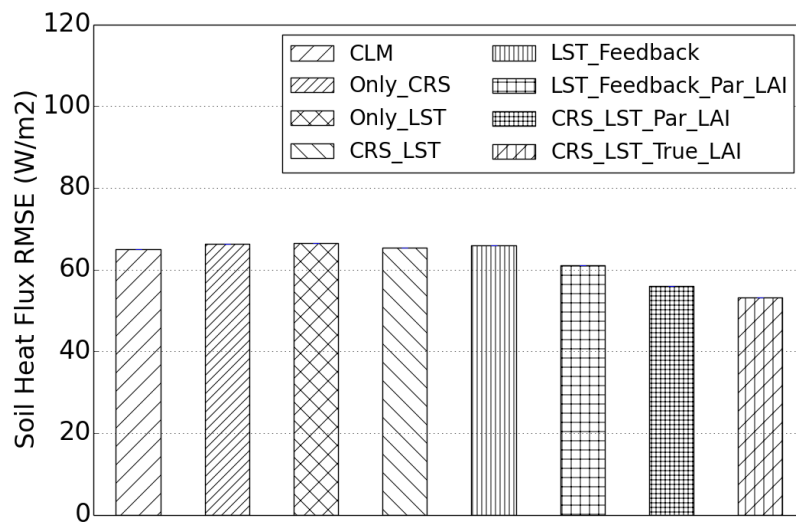
Figure 5. Evapotranspiration estimated according different scenarios for the period June-August 2012. For a full description see Fig. 3.



774



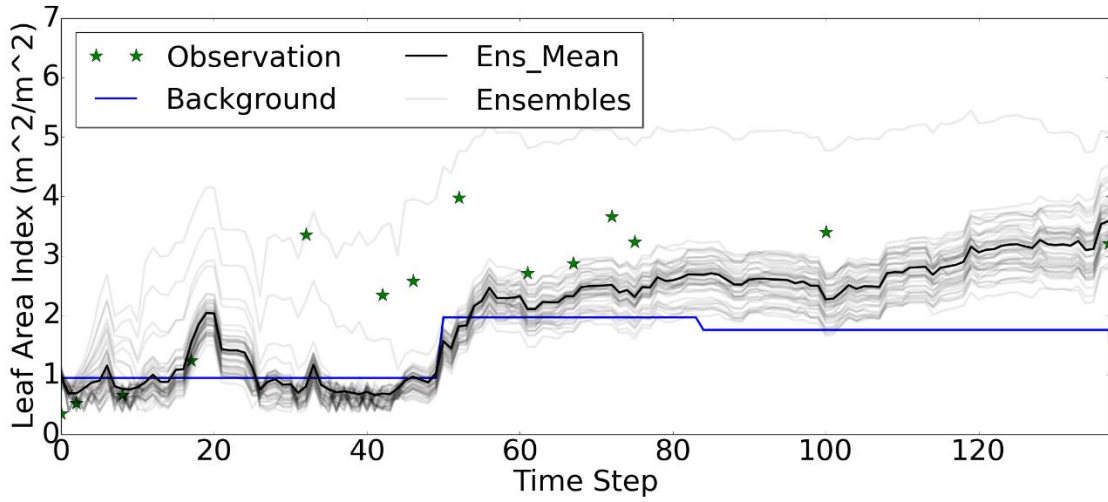
775



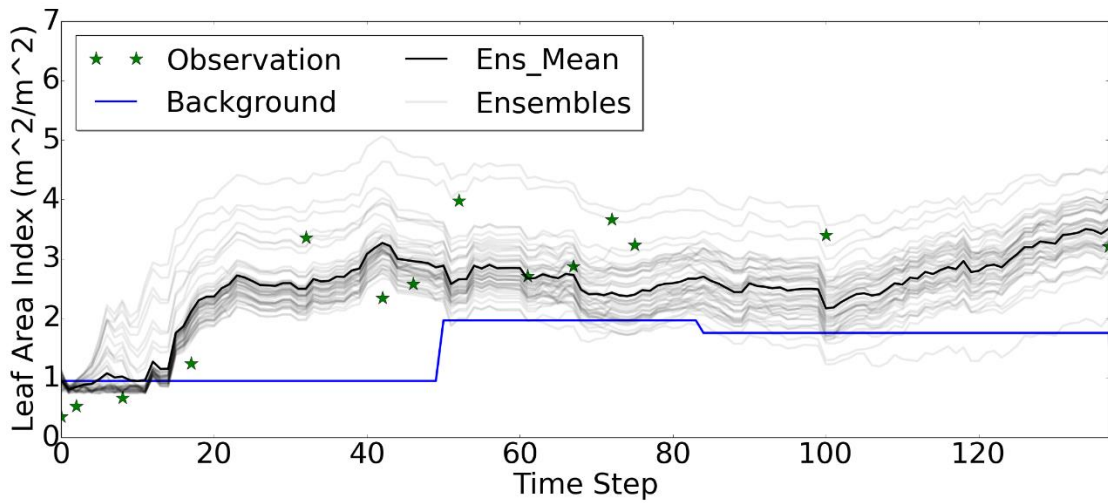
776

777 Figure 6. RMSE values of latent heat flux, sensible heat flux and soil heat flux for the
 778 period June-August 2012. For a description of the scenarios see section 3 of the paper.

779



780



781

782 Figure 7. LAI evolution for the period June-August 2012. Displayed are the measured
 783 LAI (Observation), default values (Background), mean of ensemble members
 784 (Ens_Mean) and ensemble members (Ensembles) for scenarios of
 785 LST_Feedback_Par_LAI (upper) and CRS_LST_Par_LAI (lower)

786

787

788 **References:**

- 789 Anderson, M. C., Norman, J. M., Kustas, W. P., Li, F., Prueger, J. H., and Mecikalski, J. R.: Effects of
790 Vegetation Clumping on Two-Source Model Estimates of Surface Energy Fluxes from an Agricultural
791 Landscape during SMACEX, *J Hydrometeorol*, 6, 892-909, 2005.
- 792 Barrett, D. J. and Renzullo, L. J.: On the Efficacy of Combining Thermal and Microwave Satellite Data as
793 Observational Constraints for Root-Zone Soil Moisture Estimation C-7972-2009, *J Hydrometeorol*, 10,
794 1109-1127, 2009.
- 795 Bateni, S. M. and Entekhabi, D.: Surface heat flux estimation with the ensemble Kalman smoother:
796 Joint estimation of state and parameters, *Water Resour Res*, 48, 2012.
- 797 Bogena, H. R., Herbst, M., Huisman, J. A., Rosenbaum, U., Weuthen, A., and Vereecken, H.: Potential of
798 Wireless Sensor Networks for Measuring Soil Water Content Variability, *Vadose Zone J*, 9, 1002-1013,
799 2010.
- 800 Bogena, H. R., Huisman, J. A., Baatz, R., Hendricks Franssen, H. J., and Vereecken, H.: Accuracy of the
801 cosmic-ray soil water content probe in humid forest ecosystems: The worst case scenario, *Water*
802 *Resour Res*, 49, 5778-5791, 2013.
- 803 Bosilovich, M. G., Radakovich, J. D., da Silva, A., Todling, R., and Verter, F.: Skin temperature analysis
804 and bias correction in a coupled land-atmosphere data assimilation system, *J Meteorol Soc Jpn*, 85A,
805 205-228, 2007.
- 806 Collatz, G. J., Ball, J. T., Grivet, C., and Berry, J. A.: Physiological and Environmental-Regulation of
807 Stomatal Conductance, Photosynthesis and Transpiration - a Model That Includes a Laminar
808 Boundary-Layer, *Agr Forest Meteorol*, 54, 107-136, 1991.
- 809 Crow, W. T., Kustas, W. P., and Prueger, J. H.: Monitoring root-zone soil moisture through the
810 assimilation of a thermal remote sensing-based soil moisture proxy into a water balance model,
811 *Remote Sens Environ*, 112, 1268-1281, 2008.
- 812 Crow, W. T., van den Berg, M. J., Huffman, G. J., and Pellarin, T.: Correcting rainfall using satellite-based
813 surface soil moisture retrievals: The Soil Moisture Analysis Rainfall Tool (SMART), *Water Resour Res*, 47,
814 2011.
- 815 Das, N. N., Mohanty, B. P., Cosh, M. H., and Jackson, T. J.: Modeling and assimilation of root zone soil
816 moisture using remote sensing observations in Walnut Gulch Watershed during SMEX04, *Remote Sens*
817 *Environ*, 112, 415-429, 2008.
- 818 De Lannoy, G. J. M., Houser, P. R., Pauwels, V. R. N., and Verhoest, N. E. C.: State and bias estimation
819 for soil moisture profiles by an ensemble Kalman filter: Effect of assimilation depth and frequency,
820 *Water Resour Res*, 43, n/a-n/a, 2007.
- 821 De Lannoy, G. J. M., Reichle, R. H., Arsenault, K. R., Houser, P. R., Kumar, S., Verhoest, N. E. C., and
822 Pauwels, V. R. N.: Multiscale assimilation of Advanced Microwave Scanning Radiometer-EOS snow
823 water equivalent and Moderate Resolution Imaging Spectroradiometer snow cover fraction
824 observations in northern Colorado, *Water Resour Res*, 48, 2012.
- 825 Dee, D. P.: Bias and data assimilation, *Q J Roy Meteor Soc*, 131, 3323-3343, 2005.
- 826 Desilets, D. and Zreda, M.: Footprint diameter for a cosmic-ray soil moisture probe: Theory and Monte
827 Carlo simulations, *Water Resour Res*, 49, 3566-3575, 2013.
- 828 Desilets, D., Zreda, M., and Ferré, T. P. A.: Nature's neutron probe: Land surface hydrology at an elusive
829 scale with cosmic rays, *Water Resour. Res.*, 46, W11505, 2010.
- 830 Draper, C. S., Mahfouf, J. F., and Walker, J. P.: Root zone soil moisture from the assimilation of
831 screen-level variables and remotely sensed soil moisture, *J Geophys Res-Atmos*, 116, 2011.

832 Entekhabi, D., Njoku, E. G., O'Neill, P. E., Kellogg, K. H., Crow, W. T., Edelstein, W. N., Entin, J. K.,
833 Goodman, S. D., Jackson, T. J., Johnson, J., Kimball, J., Piepmeier, J. R., Koster, R. D., Martin, N.,
834 McDonald, K. C., Moghaddam, M., Moran, S., Reichle, R., Shi, J. C., Spencer, M. W., Thurman, S. W.,
835 Tsang, L., and Van Zyl, J.: The Soil Moisture Active Passive (SMAP) Mission, *P IEEE*, 98, 704-716, 2010.
836 Evensen, G.: The ensemble Kalman filter: Theoretical formulation and practical implementation,
837 *Ocean Dynam*, 53, 343-367, 2003.
838 Franz, T. E., Zreda, M., Ferre, T. P. A., Rosolem, R., Zweck, C., Stillman, S., Zeng, X., and Shuttleworth, W.
839 J.: Measurement depth of the cosmic ray soil moisture probe affected by hydrogen from various
840 sources, *Water Resour Res*, 48, 2012.
841 Franz, T. E., Zreda, M., Rosolem, R., and Ferre, T. P. A.: A universal calibration function for
842 determination of soil moisture with cosmic-ray neutrons, *Hydrology and Earth System Sciences*, 17,
843 453-460, 2013.
844 Ghent, D., Kaduk, J., Remedios, J., Ardo, J., and Balzter, H.: Assimilation of land surface temperature
845 into the land surface model JULES with an ensemble Kalman filter, *J Geophys Res-Atmos*, 115, 2010.
846 Ghilain, N., Arboleda, A., Sepulcre-Canto, G., Batelaan, O., Ardo, J., and Gellens-Meulenberghs, F.:
847 Improving evapotranspiration in a land surface model using biophysical variables derived from
848 MSG/SEVIRI satellite, *Hydrology and Earth System Sciences*, 16, 2567-2583, 2012.
849 Han, X., Li, X., Franssen, H. J. H., Vereecken, H., and Montzka, C.: Spatial horizontal correlation
850 characteristics in the land data assimilation of soil moisture, *Hydrology and Earth System Sciences*, 16,
851 1349-1363, 2012.
852 Han, X. J., Franssen, H. J. H., Li, X., Zhang, Y. L., Montzka, C., and Vereecken, H.: Joint Assimilation of
853 Surface Temperature and L-Band Microwave Brightness Temperature in Land Data Assimilation,
854 *Vadose Zone J*, 12, 0, 2013.
855 Han, X. J., Franssen, H. J. H., Montzka, C., and Vereecken, H.: Soil moisture and soil properties
856 estimation in the Community Land Model with synthetic brightness temperature observations, *Water*
857 *Resour Res*, 50, 6081-6105, 2014a.
858 Han, X. J., Jin, R., Li, X., and Wang, S. G.: Soil Moisture Estimation Using Cosmic-Ray Soil Moisture
859 Sensing at Heterogeneous Farmland, *IEEE Geoscience and Remote Sensing Letters*, 11, 1659-1663,
860 2014b.
861 Hunt, B. R., Kostelich, E. J., and Szunyogh, I.: Efficient data assimilation for spatiotemporal chaos: A
862 local ensemble transform Kalman filter, *Physica D: Nonlinear Phenomena*, 230, 112-126, 2007.
863 Jarlan, L., Balsamo, G., Lafont, S., Beljaars, A., Calvet, J. C., and Mougou, E.: Analysis of leaf area index
864 in the ECMWF land surface model and impact on latent heat and carbon fluxes: Application to West
865 Africa, *J Geophys Res-Atmos*, 113, 2008.
866 Jin, R., Li, X., Yan, B., Li, X., Luo, W., Ma, M., Guo, J., Kang, J., Zhu, Z., and Zhao, S.: A Nested
867 Ecohydrological Wireless Sensor Network for Capturing the Surface Heterogeneity in the Midstream
868 Areas of the Heihe River Basin, China, *IEEE Geoscience and Remote Sensing Letters*, PP, 1-5, 2014.
869 Jin, R., Wang, X., Kang, J., Wang, Z., Dong, C., and Li, D.: HiWATER: SoilNET observation dataset in the
870 middle reaches of the Heihe river basin, Heihe Plan Science Data Center, doi:
871 10.3972/hiwater.120.2013.db
872 doi:10.3972/hiwater.120.2013.db, 2013. 2013.
873 Kerr, Y. H., Waldteufel, P., Wigneron, J. P., Delwart, S., Cabot, F., Boutin, J., Escorihuela, M. J., Font, J.,
874 Reul, N., Gruhier, C., and Others: The SMOS Mission: New Tool for Monitoring Key Elements of the
875 Global Water Cycle, *P IEEE*, 98, 666-687, 2010.

876 Kumar, S. V., Reichle, R. H., Harrison, K. W., Peters-Lidard, C. D., Yatheendradas, S., and Santanello, J. A.:
877 A comparison of methods for a priori bias correction in soil moisture data assimilation, *Water Resour*
878 *Res*, 48, n/a-n/a, 2012.

879 Kumar, S. V., Reichle, R. H., Koster, R. D., Crow, W. T., and Peters-Lidard, C. D.: Role of Subsurface
880 Physics in the Assimilation of Surface Soil Moisture Observations, *J Hydrometeorol*, 10, 1534-1547,
881 2009.

882 Kustas, W. and Anderson, M.: Advances in thermal infrared remote sensing for land surface modeling,
883 *Agr Forest Meteorol*, 149, 2071-2081, 2009.

884 Li, C. and Ren, L.: Estimation of Unsaturated Soil Hydraulic Parameters Using the Ensemble Kalman
885 Filter, *Vadose Zone J*, 10, 1205, 2011.

886 Li, F. Q., Crow, W. T., and Kustas, W. P.: Towards the estimation root-zone soil moisture via the
887 simultaneous assimilation of thermal and microwave soil moisture retrievals, *Adv Water Resour*, 33,
888 201-214, 2010.

889 Li, X., Cheng, G. D., Liu, S. M., Xiao, Q., Ma, M. G., Jin, R., Che, T., Liu, Q. H., Wang, W. Z., Qi, Y., Wen, J.
890 G., Li, H. Y., Zhu, G. F., Guo, J. W., Ran, Y. H., Wang, S. G., Zhu, Z. L., Zhou, J., Hu, X. L., and Xu, Z. W.:
891 Heihe Watershed Allied Telemetry Experimental Research (HiWATER): Scientific Objectives and
892 Experimental Design, *B Am Meteorol Soc*, 94, 1145-1160, 2013.

893 Miyoshi, T. and Yamane, S.: Local Ensemble Transform Kalman Filtering with an AGCM at a T159/L48
894 Resolution, *Mon Weather Rev*, 135, 3841-3861, 2007.

895 Montzka, C., Grant, J. P., Moradkhani, H., Franssen, H. J. H., Weihermuller, L., Drusch, M., and
896 Vereecken, H.: Estimation of Radiative Transfer Parameters from L-Band Passive Microwave Brightness
897 Temperatures Using Advanced Data Assimilation, *Vadose Zone J*, 12, 2013.

898 Moradkhani, H., Sorooshian, S., Gupta, H. V., and Houser, P. R.: Dual state-parameter estimation of
899 hydrological models using ensemble Kalman filter, *Adv Water Resour*, 28, 135-147, 2005.

900 Nie, S., Zhu, J., and Luo, Y.: Simultaneous estimation of land surface scheme states and parameters
901 using the ensemble Kalman filter: identical twin experiments, *Hydrology and Earth System Sciences*,
902 15, 2437-2457, 2011.

903 Oleson, K., Lawrence, D. M., Bonan, G., Drewniak, B., Huang, M., Koven, C. D., Levis, S., Li, F., Riley, W.
904 J., Subin, Z. M., Swenson, S. C., Thornton, P. E., Bozbiyik, A., Fisher, B. E. A., Kluzek, E., Lamarque, J. F.,
905 Lawrence, P. J., Leung, L. R., Lipscomb, W., Muszala, S., Ricciuto, D. M., Sacks, W., Sun, Y., Tang, J., and
906 Yang, Z.-L.: Technical Description of version 4.5 of the Community Land Model (CLM), *Ncar Technical*
907 *Note NCAR/TN-503+STR*, National Center for Atmospheric Research, Boulder, CO, 422 pp., 2013. 2013.

908 Pauwels, V. R. N., Balenzano, A., Satalino, G., Skriver, H., Verhoest, N. E. C., and Mattia, F.: Optimization
909 of Soil Hydraulic Model Parameters Using Synthetic Aperture Radar Data: An Integrated
910 Multidisciplinary Approach, *IEEE T Geosci Remote*, 47, 455-467, 2009.

911 Reichle, R. H.: Data assimilation methods in the Earth sciences, *Adv Water Resour*, 31, 1411-1418,
912 2008.

913 Reichle, R. H., Kumar, S. V., Mahanama, S. P. P., Koster, R. D., and Liu, Q.: Assimilation of
914 Satellite-Derived Skin Temperature Observations into Land Surface Models, *J Hydrometeorol*, 11,
915 1103-1122, 2010.

916 Robinson, D. A., Jones, S. B., Wraith, J. M., Or, D., and Friedman, S. P.: A Review of Advances in
917 Dielectric and Electrical Conductivity Measurement in Soils Using Time Domain Reflectometry, *Vadose*
918 *Zone J*, 2, 444-475, 2003.

919 Rodell, M., Houser, P. R., Jambor, U., Gottschalck, J., Mitchell, K., Meng, C. J., Arsenault, K., Cosgrove,

920 B., Radakovich, J., Bosilovich, M., Entin, J. K., Walker, J. P., Lohmann, D., and Toll, D.: The global land
921 data assimilation system, *B Am Meteorol Soc*, 85, 381+, 2004.

922 Rosolem, R., Hoar, T., Arellano, A., Anderson, J. L., Shuttleworth, W. J., Zeng, X., and Franz, T. E.:
923 Assimilation of near-surface cosmic-ray neutrons improves summertime soil moisture profile
924 estimates at three distinct biomes in the USA, *Hydrol. Earth Syst. Sci. Discuss.*, 11, 5515-5558, 2014.

925 Rosolem, R., Shuttleworth, W. J., Zreda, M., Franz, T. E., Zeng, X., and Kurc, S. A.: The Effect of
926 Atmospheric Water Vapor on Neutron Count in the Cosmic-Ray Soil Moisture Observing System, *J*
927 *Hydrometeorol*, 14, 1659-1671, 2013.

928 Savitzky, A. and Golay, M. J. E.: Smoothing and Differentiation of Data by Simplified Least Squares
929 Procedures, *Analytical Chemistry*, 36, 1627-1639, 1964.

930 Schwinger, J., Kollet, S. J., Hoppe, C. M., and Elbern, H.: Sensitivity of Latent Heat Fluxes to Initial
931 Values and Parameters of a Land-Surface Model, *Vadose Zone J*, 9, 984-1001, 2010.

932 Shangguan, W., Dai, Y., Liu, B., Zhu, A., Duan, Q., Wu, L., Ji, D., Ye, A., Yuan, H., Zhang, Q., Chen, D.,
933 Chen, M., Chu, J., Dou, Y., Guo, J., Li, H., Li, J., Liang, L., Liang, X., Liu, H., Liu, S., Miao, C., and Zhang, Y.:
934 A China data set of soil properties for land surface modeling, *J Adv Model Earth Sy*, 5, 212-224, 2013.

935 Shuttleworth, J., Rosolem, R., Zreda, M., and Franz, T. E.: The COsmic-ray Soil Moisture Interaction
936 Code (COSMIC) for use in data assimilation, *Hydrology and Earth System Sciences*, 17, 3205-3217,
937 2013.

938 Sun, W. X., Liang, S. L., Xu, G., Fang, H. L., and Dickinson, R.: Mapping plant functional types from
939 MODIS data using multisource evidential reasoning, *Remote Sens Environ*, 112, 1010-1024, 2008.

940 van den Hurk, B. J. J. M.: Impact of leaf area index seasonality on the annual land surface evaporation
941 in a global circulation model, *Journal of Geophysical Research*, 108, 2003.

942 Wan, Z. and Li, Z. L.: Radiance - based validation of the V5 MODIS land - surface temperature product,
943 *Int J Remote Sens*, 29, 5373-5395, 2008.

944 Xu, T. R., Liang, S. L., and Liu, S. M.: Estimating turbulent fluxes through assimilation of geostationary
945 operational environmental satellites data using ensemble Kalman filter, *J Geophys Res-Atmos*, 116,
946 2011.

947 Xu, Z. W., Liu, S. M., Li, X., Shi, S. J., Wang, J. M., Zhu, Z. L., Xu, T. R., Wang, W. Z., and Ma, M. G.:
948 Intercomparison of surface energy flux measurement systems used during the HiWATER-MUSOEXE, *J*
949 *Geophys Res-Atmos*, 118, 13140-13157, 2013.

950 Yang, K., Koike, T., Kaihotsu, I., and Qin, J.: Validation of a Dual-Pass Microwave Land Data Assimilation
951 System for Estimating Surface Soil Moisture in Semiarid Regions, *J Hydrometeorol*, 10, 780-793, 2009.

952 Yang, Z. L., Dai, Y., Dickinson, R. E., and Shuttleworth, W. J.: Sensitivity of ground heat flux to
953 vegetation cover fraction and leaf area index, *J Geophys Res-Atmos*, 104, 19505-19514, 1999.

954 Zhu, C. Y., Byrd, R. H., Lu, P. H., and Nocedal, J.: Algorithm 778: L-BFGS-B: Fortran subroutines for
955 large-scale bound-constrained optimization, *Acm Transactions on Mathematical Software*, 23, 550-560,
956 1997.

957 Zreda, M., Desilets, D., Ferre, T. P. A., and Scott, R. L.: Measuring soil moisture content non-invasively
958 at intermediate spatial scale using cosmic-ray neutrons, *Geophys Res Lett*, 35, L21402, 2008.

959 Zreda, M., Shuttleworth, W. J., Zeng, X., Zweck, C., Desilets, D., Franz, T. E., and Rosolem, R.: COSMOS:
960 the COsmic-ray Soil Moisture Observing System, *Hydrology and Earth System Sciences*, 16, 4079-4099,
961 2012.

962